Nonlinear Equilibration of Two-Dimensional Eady Waves: A New Perspective

STEPHEN T. GARNER AND NOBORU NAKAMURA

Program in Atmospheric and Oceanic Sciences, Princeton University, Princeton, New Jersey

ISAAC M. HELD

Geophysical Fluid Dynamics Laboratory/NOAA, Princeton, New Jersey

(Manuscript received 14 August 1991, in final form 31 January 1992)

ABSTRACT

The equilibration of two-dimensional baroclinic waves differs fundamentally from equilibration in three dimensions because two-dimensional eddies cannot develop meridional temperature or velocity structure. It was shown in an earlier paper that frontogenesis together with diffusive mixing in a two-dimensional Eady wave brings positive potential vorticity (PV) anomalies deep into the atmosphere from both boundaries and allows the disturbance to settle into a steady state without meridional gradients. Here we depart from the earlier explanation of this equilibration and associate the PV intrusions with essentially the same kind of vortex "roll-up" that characterizes the evolution of barotropic shear layers.

To avoid subgrid turbulence parameterizations and computational diffusion, the analogy is developed using Eady's generalized baroclinic instability problem. Eady's generalized model has two semi-infinite regions of large PV surrounding a layer of relatively small PV. Without boundaries, frontal collapse, or strong diffusion the model still produces equilibrated states, with structure similar to the vortex streets that emerge from unstable barotropic shear layers. The similarity is greatest when the baroclinic development is viewed in isentropic coordinates. The contrast between the present equilibrated solutions, which exhibit no vertical tilt, and Blumen's diffusive frontogenesis model, which allows the wave to retain its phase tilt, is briefly discussed.

1. Introduction

The finite-amplitude equilibration of two-dimensional baroclinic waves was described and analyzed by Nakamura and Held (1989, hereafter NH) using a primitive equation numerical model and Eady's basic state. According to semigeostrophic theory (Hoskins and Bretherton 1972), an unstable Eady wave should grow exponentially until the time of frontal collapse, when the standard theory becomes invalid. Thereafter, according to NH's numerical solutions, the vertical phase tilt responsible for growth begins to decrease and the eddy energy stops growing. To explain this equilibration, NH noted that the net effect of diffusion is to increase the zonal-mean potential vorticity (PV) at all levels. In semigeostrophic dynamics, the ambient PV controls wave growth through its effect on the depth of influence of boundary anomalies and on the ability of the anomalies to counterpropagate against the shear. The analogous dependence on ambient static stability was invoked by Gall (1976) in his proposed quasigeostrophic equilibration scenario. Based on the semigeostrophic dynamics, NH attributed the termination of wave growth indirectly to the increase in zonal-mean PV.

It is clear from NH's results that the generation of positive PV anomaly in Eady life-cycle simulations is due to horizontal diffusion of heat in occluding frontal zones. The possibility that frontogenesis could be the primary agency for baroclinic wave equilibration was mentioned earlier by Orlanski (1986), although his specific mechanisms involved energy dissipation through turbulence or nongeostrophic waves, rather than PV generation. While there is little doubt that PV generation is involved in the equilibration, we see two problems with the final part of NH's explanation. Both of these are evident in the PV field, shown in Fig. 1, near the time of maximum eddy energy.[1] First of all, the positive PV anomaly has not become homogenized enough to have produced a global change in the internal depth scale by the time the wave has begun to equilibrate. Second, the separation between the rigid boundaries is probably dynamically irrelevant once tongues of large PV extend well inside the domain. By then, the PV tongues themselves can interact with each other.

A more appropriate—and in many ways simpler—

Corresponding author address: Dr. Stephen T. Garner, Princeton University, Program in Atmospheric and Oceanic Sciences, Geophysical Fluid Dynamics Laboratory, Princeton, NJ 08542.

[1] The evaluation of Ertel potential vorticity for this figure corrects a quantitative error in NH.

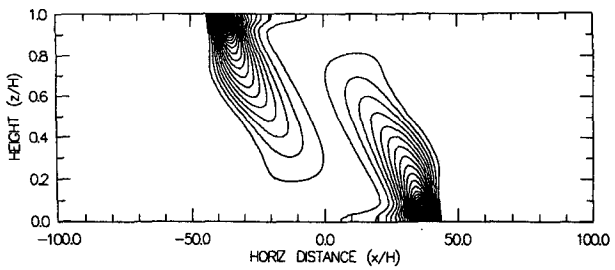

FIG. 1. Ertel potential vorticity in a finite-amplitude Eady wave generated by a primitive equation numerical model. Solution is near the time of maximum eddy energy. Contour interval is $5q_0$ (zero suppressed), where q_0 is the initial PV. The Rossby radius [defined $(q_0/f^3)^{1/2}H$] and wavelength are $100H$ and $400H$, respectively.

view of the equilibration begins to emerge as the rigid boundaries are deemphasized. In NH, diffusion was viewed as tapping the PV "reservoirs" that may be considered implicit within the boundaries. Here we propose to describe the equilibration as a "rollup" of the relatively low-PV air mass confined between the reservoirs. This terminology is based on an analogy with the rollup of barotropic shear layers into isolated vortices. A typical barotropic rollup is shown in Fig. 2, which is taken from a study by Pozrikidis and Higdon (1985). (The barotropic model will be described more fully in section 2.) Growth of the eddy energy culminates as the relatively small vorticity of the exterior layers invades and spans the interior layer of relatively large vorticity. Eventually, isolated vortices emerge. It is clear that equilibration through vortex roll up cannot be described in terms of linear waves propagating in a modified mean flow.

The baroclinic–barotropic analogy is not self-evident in all of its details. For example, the interfaces between PV layers in the baroclinic model have two dimensions rather than one. The analogy becomes clearer when the baroclinic development is viewed in isentropic coordinates. On isentropic surfaces, the basic state has meridional structure and the boundaries between PV regions appear as one-dimensional interfaces. As we will see, the imposed two-dimensionality of the disturbance makes all such surfaces identical insofar as the perturbations are concerned. The PV is closely analogous, in this context, to the negative reciprocal of the barotropic vorticity.

In order to reduce the ambiguity associated with frontal collapse and diffusion, we consider the baroclinic development in the context of a generalized model of baroclinic instability. The more general model, diagrammed in Fig. 3, contains two semi-infinite, uniform-PV regions surrounding a layer with smaller PV. There are no geometric boundaries to deal with. This "three-regime" model was introduced by Eady (1949), who suggested that it might apply to elevated cloud layers. In the limit where the outer regions have infinite potential vorticity, the interfaces become dynamically rigid and the more familiar Eady model is recovered. For comparison, Fig. 3 includes a diagram

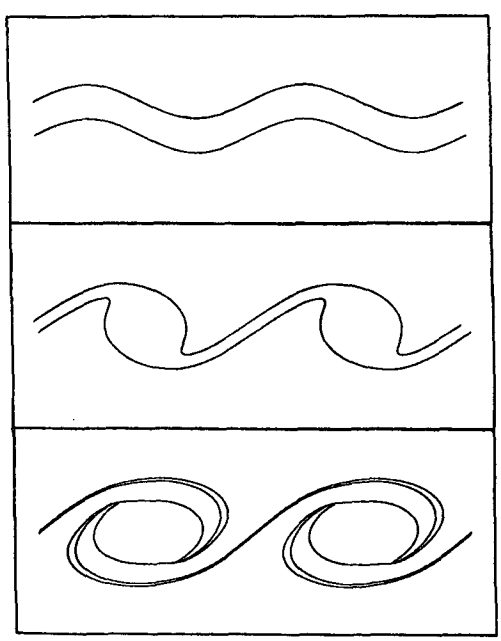

FIG. 2. Evolution of vortex layer disturbed at wavenumber $k = 1.0$. Times are (top) $t = 0$, (middle) $t = 6$, and (bottom) $t = 15$. (From Pozrikidis and Higdon 1985; wavenumber and time are scaled by the width and vorticity of the layer.)

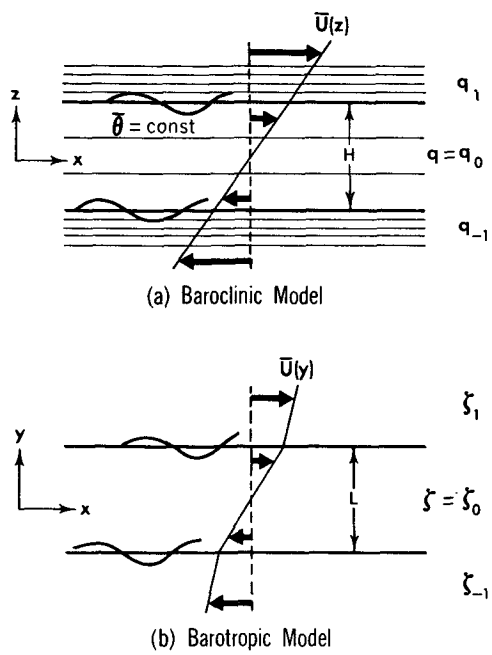

FIG. 3. Diagrams of the (a) baroclinic and (b) barotropic models used in this study. Symmetric distributions of vorticity and potential vorticity are shown. The horizontal surfaces in (a) are the undisturbed isentropes.

of the barotropic shear-layer problem. The classical problem considered by Rayleigh (1894) has been generalized by allowing the two outer layers to have arbitrary (not necessarily zero) vorticity.

In section 2, we obtain nondiffusive numerical solutions of the generalized baroclinic instability problem, and concentrate on the finite-amplitude behavior. In section 3, isentropic coordinates are introduced in order to make a cleaner comparison between the baroclinic and barotropic problems. The discussion in section 4 is concerned mainly with how the diffusive frontogenesis model proposed by Blumen (1990) compares with the present view of finite-amplitude Eady waves.

2. Unbounded models of baroclinic instability

a. Linear properties

The baroclinic and barotropic instabilities that we are comparing are of the "inflectional" type, most naturally understood as an interaction between counterpropagating edge waves (Hoskins et al. 1985; Sakai 1989). Potential vorticity discontinuities support baroclinic edge waves in much the same way as vorticity jumps support barotropic ones. In a quasigeostrophic model, vertical PV jumps are represented as sheets of infinite "pseudo-PV" anomaly. The integrated strength of these sheets varies linearly in the meridional direction. The Charney–Stern (1962) necessary condition for instability is satisfied if the middle layer has either a maximum or a minimum of PV, but Fjørtoft's (1950) theorem requires that it be a minimum in order for the meridional pseudo-PV gradients on the interfaces to be positively correlated with the zonal velocity.

To see that the necessary configuration is actually unstable, we solve for the quasigeostrophic normal modes. For simplicity, consider an incompressible, Boussinesq fluid. The perturbation geostrophic streamfunction ϕ is then a solution of (e.g., Pedlosky 1987, section 6.8)

$$\phi_{xx} + [(f^2/N^2)\phi_z]_z = Q'_{qg}/f, \qquad (1)$$

where $N^2(z)$ is the basic static stability and f is the Coriolis parameter. The quantity Q'_{qg} is what was referred to above as pseudo-PV anomaly. The meridional velocity component v'_g and potential temperature anomaly θ' (reference value θ_0) are related to the streamfunction by $\phi_x = fv'_g$ and $\phi_z = g\theta'/\theta_0 \equiv b'$. Since pseudo PV is conserved following the geostrophic motion, the perturbation is governed by

$$(\partial/\partial t + \bar{u}\partial/\partial x)Q'_{qg} = v'_g(\partial/\partial z)(f^4\Lambda/N^2), \quad (2)$$

where the basic flow is $\bar{u} = \Lambda z$, with $b = N^2 z - f\Lambda y$. Since N^2 is uniform in the layers, it follows that normal modes have $Q'_{qg} = 0$ everywhere except at the interfaces.

The perturbation streamfunction must be bounded at infinity and continuous at the interfaces. The other interface condition is derived from the conservation of potential temperature and the continuity of the vertical velocity. For a QG disturbance, the virtual interface displacement, δ, is related to the vertical velocity, w, by $w = (\partial/\partial t + \bar{u}\partial/\partial x)\delta$. The potential temperature equation is then

$$(\partial/\partial t + \bar{u}\partial/\partial x)(b' + N^2\delta) = \Lambda\phi_x, \quad z = \pm H/2, \quad (3)$$

where H is the depth of the middle layer. For continuity of ϕ, we must have $\delta(x, t) = -\Delta b'/\Delta(N^2)$, with Δ indicating an interfacial jump.

The dispersion relation for normal modes of the problem (1)–(3) is derived in appendix A. Growth rates for symmetric distributions of N^2 are shown in Fig. 4 for several choices of the ratio between values of N^2 in the inner and outer layers. Defining $\bar{q} = fN^2$ as the basic potential vorticity, we refer to these values as q_0/f and $q_{\pm 1}/f$, respectively (cf. Fig. 2a). Linear instability requires that $q_0/q_{\pm 1} < 1$, according to the theorems cited at the beginning of the section. The standard Eady model ($q_0/q_{\pm 1} = 0$) is the most unstable, with a maximum growth rate of $\sigma_m = 0.31$ at $k = 1.61$ and a shortwave cutoff at $k_c = 2.40$ [k and σ are normalized by $(f^3/q_0)^{1/2}H^{-1}$ and $(\Lambda^2 f/q_0)^{1/2}f$, respectively]. The cutoff wavenumber is most sensitive to the PV ratio when the latter is small, whereas the maximum growth rate changes most rapidly as the PV ratio approaches unity.

Also shown in Fig. 4 are growth rates for the linearized barotropic problem mentioned in the Introduction (cf. Fig. 2b) and solved in appendix A. Results in the figure are for symmetric distributions of the vorticity,

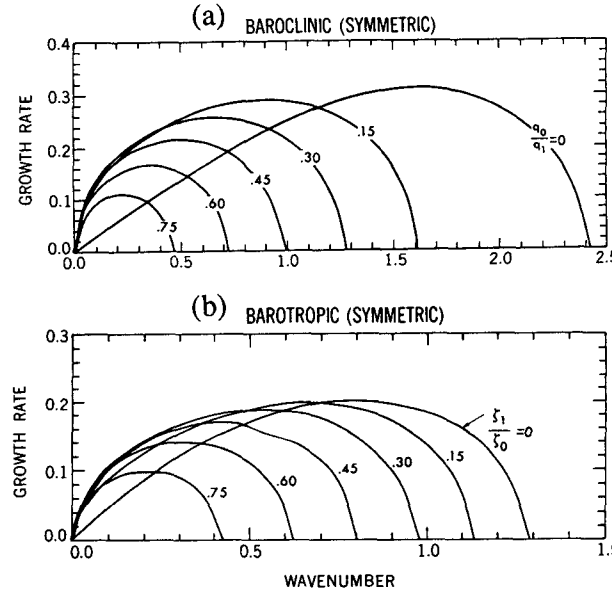

FIG. 4. Growth rate vs wavenumber in the symmetric (a) baroclinic and (b) barotropic models for different ratios of inner-to-outer vorticity or PV. Growth rate and wavenumber are scaled by $f/\mathrm{Ri}^{1/2}$ and L^{-1}, where $\mathrm{Ri} \equiv q_0/(f\Lambda^2)$ and $L \equiv (q_0/f^3)^{1/2}H$. For the symmetric basic states, the unstable modes move with the vertically averaged basic flow, irrespective of wavenumber.

$\bar{\zeta} = -d\bar{u}/dy$; that is, $\zeta_1 = \zeta_{-1}$. The necessary conditions for instability are satisfied if $|\zeta_{\pm 1}/\zeta_0| < 1$ (k and σ are normalized by L^{-1}, where L is the middle-layer width, and ζ_0, respectively). The barotropic problem differs mathematically because of the constancy of the coefficients in the diagnostic equation for perturbation vorticity,

$$\psi_{xx} + \psi_{yy} = \zeta', \tag{4}$$

which is the counterpart of (1). Corresponding to (2), we have

$$(\partial/\partial t + \bar{u}\,\partial/\partial x)\zeta' = -v'(\partial/\partial y)\bar{\zeta}. \tag{5}$$

In normal-mode solutions, $\zeta' = 0$ within the layers of uniform $\bar{\zeta}$.

The barotropic problem also has a simpler relationship between the virtual interface displacement, say $\eta(x, t)$, and the perturbation streamfunction ψ. Since the velocity perturbation is $(u', v') = (-\psi_y, \psi_x)$, the zonal momentum equation and continuity of pressure imply

$$(\partial/\partial t + \bar{u}\,\partial/\partial x)\eta = \psi_x, \quad y = \pm L/2, \tag{6}$$

where $\eta \equiv -\Delta(\psi_y)/\Delta\bar{\zeta}$. The case $|\zeta_{\pm 1}/\zeta_0| = 0$, analogous to $q_0/q_{\pm 1} = 0$, is the most unstable, with $\sigma_m = 0.20$ at $k = 0.79$ and a cutoff at $k_c = 1.28$.

There is a way to rewrite the baroclinic matching condition (3) in a symmetric form like (6). It can be shown—either by manipulating (3) or by integrating (2) across the interfaces—that the baroclinic condition is equivalently

$$(\partial/\partial t + \bar{u}\,\partial/\partial x)\eta_i = \phi_x/f, \tag{7}$$

where $\eta_i \equiv \Delta(b'/N^2)/\Delta(f\Lambda/N^2)$. Note that $\delta_i \equiv -b'/N^2$ is the (linearized) vertical displacement of an isentropic surface at a fixed latitude. The denominator in the definition of η_i involves the slope, $\alpha_i \equiv f\Lambda/N^2$, of the basic isentropes. Therefore, $\eta_i = -\Delta\delta_i/\Delta\alpha_i$ is the linearized *meridional* displacement of an interface in isentropic coordinates. Since the source of differences between the barotropic and baroclinic linearized models can be confined to the coefficients in the respective streamfunction equations, we see that differences between ϕ and ψ will be noticeable only for large contrasts in vorticity and PV. The simplicity of (7) is one of the reasons why it is natural to study the two-dimensional baroclinic problem in isentropic coordinates. We will return to that approach in section 3.

b. *Finite-amplitude properties*

To study the three-regime model at finite amplitude, we avoid the standard quasigeostrophic (QG) model. In that model, two-dimensional waves do not equilibrate at all (they retain their modal structure for all time) because the vertical advection of PV anomalies is ignored. Instead, we use a numerical model based on the semigeostrophic (SG) equations (Hoskins and Bretherton 1972; Hoskins 1975), in which vertical advection includes the perturbations. In an application with large vertical PV variations, the QG and SG models are similar only at small amplitude. In the small-amplitude limit, vertical displacements of an interface in the SG model correspond to the jumps (vertical discontinuities) in perturbation temperature in the QG model. For example, a raised interface corresponds to a negative jump if N^2 is larger in the upper layer. Interface displacement appears in the linearized SG problem exactly as the virtual displacement δ appears in (3) (e.g., Blumen 1980).

The numerical model is formulated in "geostrophic" coordinates ($X = x + v_g/f$, $Y = y - u_g/f$, $Z = z$). The diagnostic equation for the perturbation streamfunction in the two-dimensional Boussinesq SG model with zonally symmetric basic state is

$$(q_{sg}/f^3)\Phi_{XX} + \Phi_{ZZ} = q'_{sg}/f, \tag{8}$$

where $\Phi \equiv \phi + \frac{1}{2}(\phi_X/f)^2$ and the *total* PV, q_{sg}, is conserved following the *total* flow (Hoskins 1975). To initialize, the two interfaces are perturbed with small sinusoidal displacements phase shifted in a manner consistent with a growing normal mode near the most unstable wavelength. The phase shift is downshear with height, like that of the potential temperature anomaly in a growing QG wave. The interfaces are subsequently moved by the combined basic flow and ageostrophic circulation. The ageostrophic streamfunction, χ, is obtained from

$$[(q_{sg}/f^3)\chi_X]_X + \chi_{ZZ} = -2\Lambda\Phi_{XX} \tag{9}$$

(Hoskins 1975). If $\delta(X, T)$ is the height of the interface (so that $d\delta/dt$ is the vertical velocity at the interface), we have $\partial\delta/\partial T = -\bar{u}\partial\delta/\partial X + w$, where T is the local time in geostrophic coordinates and $w = -\chi_X/(1 - v'_X/f)$. This gives a forecast of the interface position.

If the position of the interfaces is known, then so is $q_{sg}(X, Z)$, and a horizontally periodic solution for $\Phi(X, Z)$ can be obtained by solving (8). That solution determines the right-hand side of (9), from which $\chi(X, Z)$ and $\partial\delta/\partial T$ are then calculated. Since the interfaces are gridded in the horizontal direction, that is, $\delta = \delta(X, T)$, they cannot overturn in the XZ plane. This artificially prevents extreme filamentation and wrapping of the PV regions. The alternative is to use tracers of the two-dimensional flow to represent the interfaces, but we have not attempted that calculation. Because of the variability of the coefficient q_{sg} in (9), it is not possible to apply the methods of "contour dynamics" (e.g., Dritschel 1988; Pozrikidis and Higdon 1985) directly to the baroclinic problem.

The two streamfunctions, Φ and χ, are computed using finite differences on an 80-by-80-point grid. To meet the boundary conditions at infinity, outwardly damped vertical structures are selected for each resolved horizontal scale. The method is described more fully

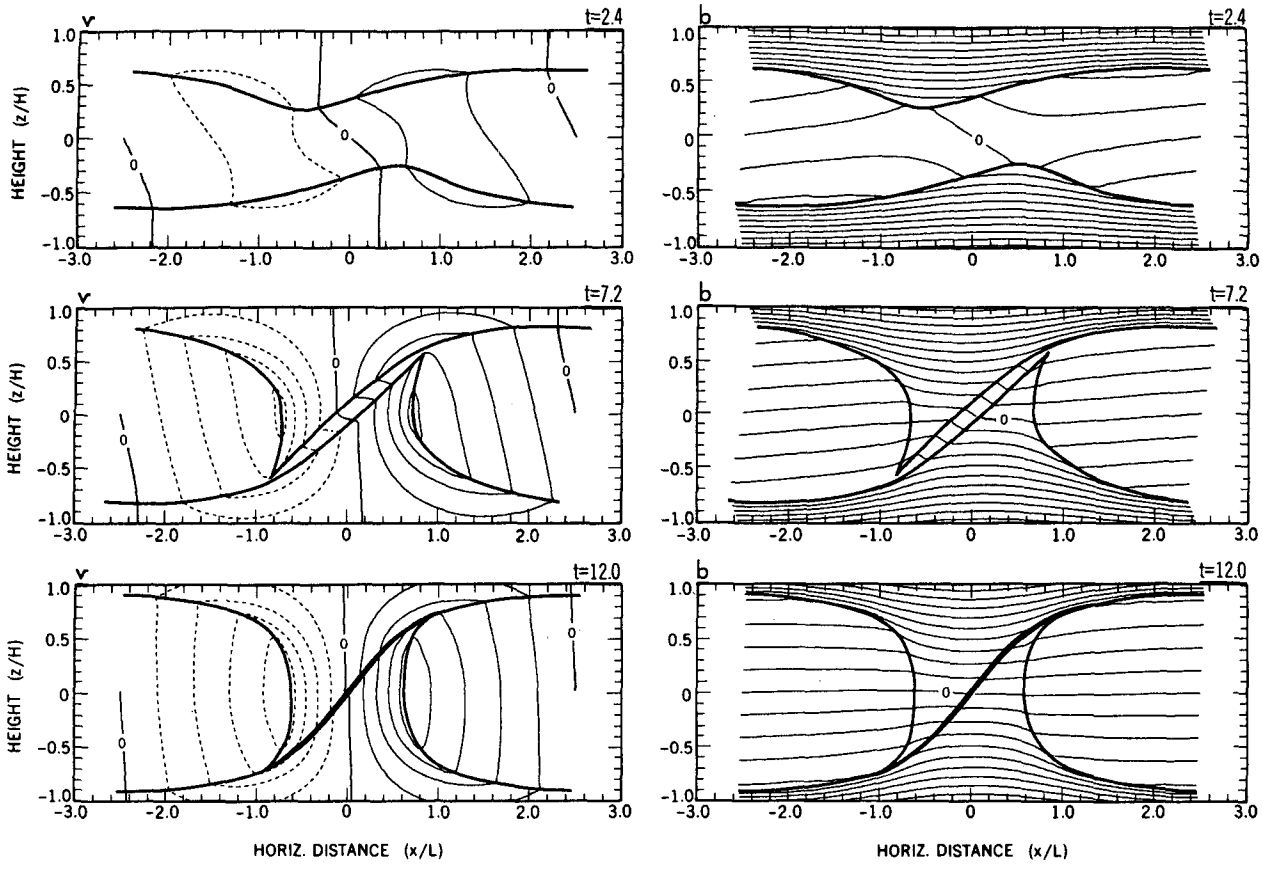

FIG. 5. Evolution of the baroclinic wave with wavenumber $k = 1.26$ (wavelength 5.0) in the semigeostrophic three-regime model with $q_1 = q_{-1} = 7q_0$. Times are (top) $t = 2.4$, (middle) $t = 7.2$, and (bottom) $t = 12.0$ (time and horizontal distance scaled as in Fig. 4). Shown are vertical cross sections in physical space of the meridional velocity v_g' (left) and the total potential buoyancy $\bar{b} + b'$ (right). The interfaces between PV regions are traced with heavy lines. The vertical axis is scaled by the undisturbed interface separation H. Contour intervals are $\delta v = 0.2(q_0/f)^{1/2}H$ and $\delta b = 0.4(q_0/f)H$.

in appendix B. The initial amplitude of the displacements is $0.1H$, where H is the undisturbed depth of the middle layer. The solutions will be shown as Y sections in physical (xz) space.[2]

The first case that we consider (Fig. 5) has equal PV values in the two outer regions, with an inner-to-outer PV ratio $q_0/q_{\pm 1} = 1/7$. The depth of the computational domain is twice the undisturbed depth of the middle PV region. There is a period of faster-than-exponential growth of the intrusions lasting until about $t = 6$ [units of $\mathrm{Ri}^{1/2}/f$, with $\mathrm{Ri} \equiv q_0/(f\Lambda^2)$], which represents about 1.5 e-folding times based on the linear analysis. This behavior is evidence that the horizontal convergence in the secondary circulation increases faster than exponentially in the cyclonic parts of the wave, as in the standard SG Eady model prior to frontal collapse. At around $t = 6$, when the intrusions have achieved the same depth as the original middle layer, the growth rate begins to decrease rapidly. By $t = 12$, the solution is essentially steady.[3]

The second case (Fig. 6) also has a symmetric PV distribution, but with stiffer interfaces, $q_0/q_{\pm 1} = 1/50$. This choice is much closer to the "Eady limit" of zero PV ratio. The computational domain for this solution is 1.5 times as deep as the undisturbed middle-layer depth. With vertical motion more inhibited near the PV jumps, the ageostrophic circulation can produce smaller horizontal scales where the interfaces fold in-

[2] The choice of cross section makes a small difference in the potential temperature plots, since $(\partial\bar{b}/\partial Z)_Y = q_{sg}/f$ while $(\partial\bar{b}/\partial z)_y = q_{sg}/f + \Lambda^2$. In order to regard the present maps of total potential temperature as y sections, one must ignore the vertical advection of $\bar{u}$ in the zonal momentum equation (so that $v = v_g$), as in the original model of Hoskins and Bretherton (1972). This technicality will come up again in section 3.

[3] Since $\delta(X)$ is single valued, the overturning of the PV interfaces in Fig. 5 shows that $(\partial x/\partial X)_s$, the partial derivative following the interface, must be changing sign. The sign changes occur on the concave side of the cusps in the intrusions and are due mainly to the vertical variation of v_g in XZ space. The horizontal derivative $(\partial x/\partial X)_Z$ is of one sign and, accordingly, the vorticity $\partial v_g/\partial x$ is finite everywhere in the present solutions.

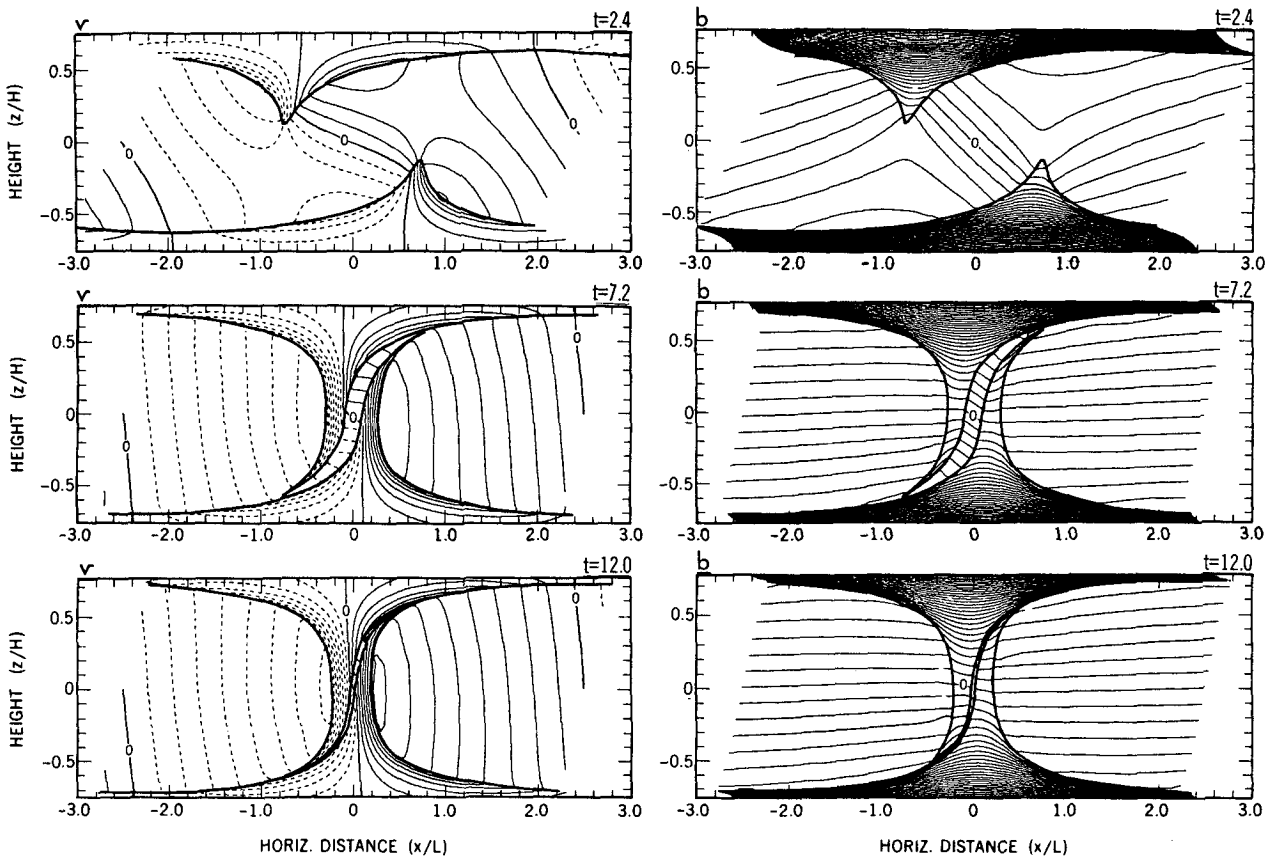

FIG. 6. As Fig. 5 but for the case $q_1 = q_{-1} = 50q_0$, and $k = 1.26$ (wavelength 5.0).

ward. The equilibration behavior, however, is qualitatively similar to the first case. Precisely because of the stiffness of the diagnostic equations with $q_{\pm 1} \gg q_0$, it is not possible to get much closer to the Eady limit with our balanced numerical model. If a unique solution exists in this limit, we expect that the intrusions will be infinitely narrow filaments supporting discontinuities of wind and temperature, qualitatively like the frontogenesis solution obtained by Cho and Koshyk (1989) using deformation forcing.

The third solution (Fig. 7) has an asymmetrical basic PV distribution, with $q_{-1}:q_0:q_1 = 50:1:7$. For simplicity, we eschew the normal mode in this case and perturb both interfaces with the same initial amplitude. The undisturbed middle layer is half as deep as the computational domain. The asymmetry of the basic state does not prevent the disturbance from becoming quasi-steady at finite amplitude. The region of large PV created by the intrusions settles down a little to the right of center (the initial perturbation is centered about $x = 0$). This is mainly because the steering level for the asymmetric linear modes is above middepth when $q_1 < q_{-1}$, as noted in appendix A (cf. Fig. 11). The difference in the widths of the lower and upper intrusions reflects the difference in stiffness of the two interfaces.

The asymmetric example can be considered a crude model of the midlatitude troposphere and stratosphere in which surface frontal collapse and/or horizontal thermal diffusion provide the possibility of narrow PV "intrusions" from below. Thus, it is closer to the gridpoint simulation by Orlanski (1986), who found a similar quasi-steady state. Intrusions of large-PV air at the lower interface differ in one important detail from occlusions in the atmosphere. The process of occlusion (e.g., Fig. 1) tends to generate large PV within strips of relatively warm air at the ground, whereas the analogous PV structures in the three-regime model contain anomalously cold air. The distinction disappears when the structures are very narrow, in which case most of the PV anomaly is due to the wind shear. We note that at early times, the upper intrusion in Fig. 7 resembles the broad tropopause lowering recently documented by Hirschberg and Fritsch (1991), although the (three-dimensional) cyclogenesis in their case comes to an end before reaching a state like that shown in the bottom panel of Fig. 7.[4]

[4] The referenced paper was pointed out to us by a reviewer.

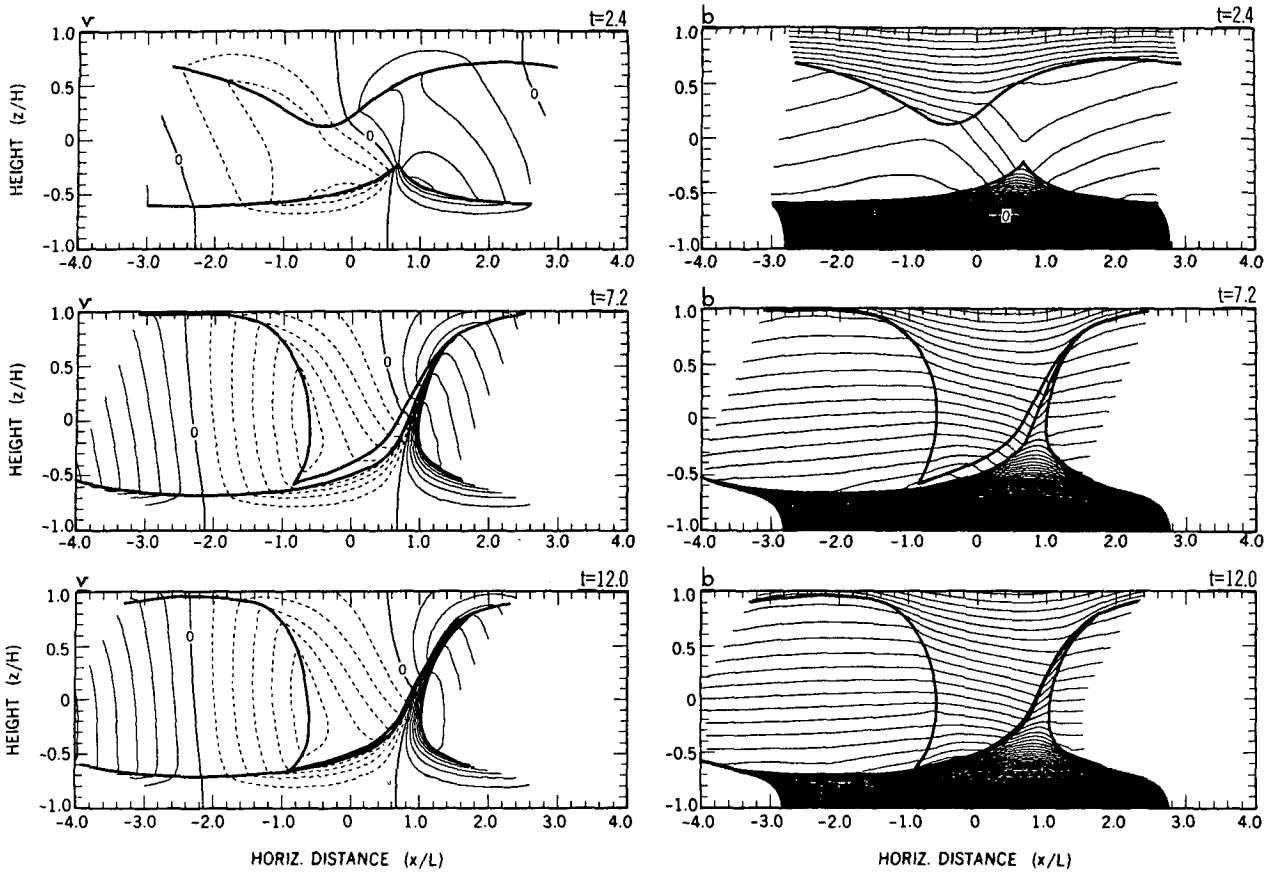

FIG. 7. As Fig. 5 but for the asymmetric case $q_1 = 7q_0$, $q_{-1} = 50q_0$ and $k = 1.12$ (wavelength 5.6).

In all of the nondiffusive solutions, the initial vertical tilt of the PV anomalies is effectively eliminated by the gradual extension of the intrusions. As this happens, the disturbance becomes more symmetrical and the PV contours can become aligned with the total flow in the xz cross section. The streamfunction for the total flow in the case $q_0/q_{\pm 1} = 1/50$ is shown in Fig. 8 at $t = 9.6$. By this time, the alignment is essentially complete (within the resolution of the model) and the "braids" connecting the isolated vortices have all but lost their dynamical importance. An analogous alignment of vorticity and streamfunction contours characterizes an equilibrated barotropic disturbance. The barotropic example in Fig. 8, shown for comparison, is from the simulation by Pozrikidis and Higdon (1985) previously seen in Fig. 2.

The numerical procedure in the referenced work allows more extensive wrapping of small-vorticity fluid around centers of large vorticity. Fundamentally, however, the barotropic state is less complicated in that the velocity anomaly is directly related to the vorticity anomaly. The baroclinic disturbance depends on a secondary (ageostrophic) circulation to keep the "tower" of large PV from being tipped over by the basic shear. The ageostrophic circulation arises to

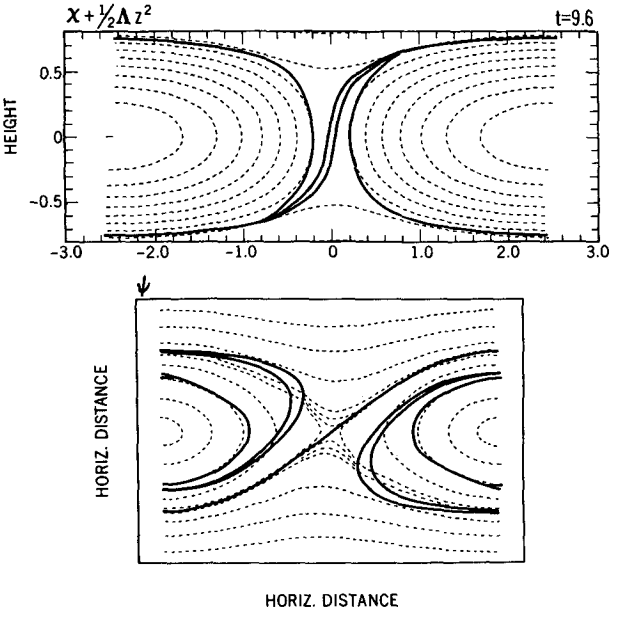

FIG. 8. Streamfunctions for the part of the flow responsible for displacing the interfaces in the (top) baroclinic case of Fig. 6 ($t = 9.6$) and (bottom) barotropic case of Fig. 2 ($t = 16.5$). Barotropic solution is from Pozrikidis and Higdon (1985).

maintain the balanced vortex against destruction by advection of perturbation wind and basic temperature. The baroclinic rollup is similar to the barotropic rollup only because the secondary circulation determined by (9) comes into phase with the relative vorticity and PV anomaly fields as the vertical phase tilt disappears. Alignment of the three-dimensional flow with the isentropic surfaces is implicit in steady baroclinic disturbances.

The present model does not reproduce the temporal oscillation of domain-averaged PV that occurs in NH's diffusive primitive equation simulation. From their sensitivity tests, it is clear that the oscillation is associated with diffusive "reabsorption" of PV anomaly into the anticyclonic parts of the boundary (which are cooled or warmed mainly by vertical fluxes). Also missing from the present simulations is the oscillation of the tilt of the PV tower, as defined by the location of the PV anomaly concentrations at the two boundaries. In the diffusive solution, these concentrations are sheared past each other, then diffused horizontally and partially reabsorbed, after the wave stops growing. An episode of relatively weak cyclogenesis, frontogenesis, and PV generation then reestablishes the original tilt. The nondiffusive model captures the time-averaged structure of the diffusive solution at large times, but eliminates a lot of the transience. Apparently, the alignment that eliminates PV advection is more elusive for complicated PV distributions and ongoing diffusion.

3. Formulation in isentropic coordinates

The similarity between the baroclinic and barotropic life cycles is obscured somewhat by the possibility of potential temperature advection in all three directions in the baroclinic problem. Changing to isentropic coordinates conceals this difference and reduces the dimensionality of the velocity field and fluid interfaces to that of the barotropic problem. Although the velocity in the isentropic baroclinic model must have a divergent component (associated with vertical stretching), the y invariance of the perturbation at constant z ensures that the disturbance looks the same on any isentropic surface. Changing to isentropic coordinates provides a better perspective on the nonlinear equilibration, especially near the "Eady limit."

The height of an undisturbed isentropic surface is $\bar{z}(y) = (f^2\Lambda/q)(y - y_i)$, where y_i is a constant for each isentrope in each uniform-PV layer. The basic flow is therefore $\bar{u}(y) = \mathrm{Ri}^{-1} f(y - y_i)$, where $\mathrm{Ri} \equiv q/(f\Lambda^2)$, the Richardson number of the layer. An unstable basic state in isentropic coordinates is depicted by the *barotropic* diagram in Fig. 2. The undisturbed profile $\bar{u}(y)$ can be reinterpreted as either $\bar{u}(y)$ or $\bar{z}(y)$. The balance approximations (QG and SG), as applied to Eady's model, are based in part on the largeness of Ri.

The momentum equations may be written, as usual, in the form

$$du/dt = f(v - v_g) \tag{10}$$

$$dv/dt = -f(u - u_g). \tag{11}$$

However, the parcel derivative is $d/dt \equiv \partial/\partial t + u\partial/\partial x + v\partial/\partial y$ and differentiation is at constant b (with the flow assumed to be adiabatic). If P is the perturbation geostrophic streamfunction, we have $(u_g', v_g') \equiv (-P_y/f, P_x/f)$. The height anomaly $z' \equiv z - \bar{z}(y, b)$ is related to the streamfunction via hydrostatic balance (e.g., McWilliams and Gent 1980):

$$P_b = -z'. \tag{12}$$

For incompressible Boussinesq motion, the xyb geostrophic streamfunction is the sum of the xyz streamfunction, say p, and the Boussinesq potential energy. Thus, $P = p - bz - \bar{P}(y, b)$. The basic state satisfies $\bar{P}_y = -f\bar{u}$ and $\bar{P}_b = -\bar{z}$. Finally, the continuity equation has the form

$$(d/dt)z_b = -(u_x + v_y)z_b. \tag{13}$$

The dependent variables in (10)–(13) are u, v, P, and z. The non-Boussinesq isentropic system, with a fifth dependent variable, is discussed by Hoskins and Draghici (1977).

The present system conserves the Boussinesq potential vorticity, $q = (z_b)^{-1}(f + v_x - u_y)$. After applying the geostrophic momentum approximation (Hoskins 1975) to (10)–(11), conservation of PV becomes $dq_{sg}/dt = 0$, where

$$q_{sg} = (z_b)^{-1}(f + v_{gx})(f - u_{gy})/f. \tag{14}$$

Since the disturbance is two-dimensional, all isentropic surfaces are the same and we are able to replace $\partial/\partial b$ by $(-1/\bar{b}_y)\partial/\partial y$. It is also helpful to nondimensionalize. In the xz plane, balanced disturbances have an aspect ratio of order $(f^3/q)^{1/2}$. Dividing by the (undisturbed) slope of the isentropes, $\alpha_i = f^2\Lambda/q$, we determine that y scales on isentropic surfaces will be greater by a factor of $\mathrm{Ri}^{1/2}$ than x scales. This anisotropy is absorbed in the scales $(x, y)\tilde{}(1, \mathrm{Ri}^{1/2})(q_0/f^3)^{1/2}H$ for horizontal distances. Since zonal and meridional advection are equally important in balanced disturbances, the velocity components should be scaled according to $(u, v)\tilde{}(1, \mathrm{Ri}^{1/2})\Lambda H$. From now on, we define $\mathrm{Ri} = q_0/(f\Lambda^2)$.

If the PV, absolute vorticity, and height are scaled by q_0, f, and H, respectively, the expression (14) for the PV in the two-dimensional, isentropic SG model becomes $q_{sg} = (z_y)^{-1}(1 + v_{gx})(1 - \mathrm{Ri}^{-1}u_{gy})$. We shall ignore the term involving u_g, since other terms of order $1/\mathrm{Ri}$ have been neglected elsewhere. The resulting quantity is the one conserved by the equations introduced by Hoskins and Bretherton (1972), in which the left-hand side of (10) is neglected (and $v = v_g$). With $v = v_g$, the horizontal divergence becomes u_x

$+ v_y = (u_a)_x$, where $u_a = -(1/f)dv_g/dt$. We continue to refer to the approximation as semigeostrophy (SG).

Conveniently, the last adjustment makes the diagnostic problem for the geostrophic motion formally linear. For a zonally symmetric basic state, the perturbation streamfunction equation [corresponding to (14)] is now

$$hP_{xx} + P_{yy} = -h'. \tag{15}$$

where P is scaled by $(q_0/f^2)H^2$ and $h \equiv q_{sg}^{-1}$. The non-Boussinesq form of h has been called the potential density (Magnusdottir and Schubert 1990). If time is scaled by $\mathrm{Ri}^{1/2}/f$, the nondimensional derivative, d/dt, expands to exactly the same expression as that following (11). Conservation of PV may be expressed as $dh/dt = 0$.

A comparison between (15) and (4) reveals a close analogy between h and $-\zeta$. Both $|\zeta|$ and $|h|$ are smallest in the outer regions of an unstable three-regime model (for stability to overturning in the y direction, h is restricted to positive values, as is the quantity $\bar{\zeta} + f$ if there is background rotation in the barotropic problem). The barotropic zonal velocity anomaly, $u' = -\psi_y$, is analogous to the isentropic height anomaly and geostrophic zonal-flow anomaly, since $z' = u_g' = -P_y$ (hydrostatic balance and definition of u_g). Thus, z' must be matched across the PV jumps in the isentropic model. At small amplitude, this is achieved by imposing (7), with $\eta_i = -\Delta z'/\Delta \bar{z}_y$, at the undisturbed interface positions (also see appendix A). The term P_{yy} in (15) corresponds to the thickness of the isentropic layers or the slope of the isentropic surfaces.

In the previous section we mentioned the necessary alignment of the ageostrophic circulation with the PV contours and interfaces. From (10)–(12), it is straightforward to derive the isentropic form of the Sawyer–Eliassen equations, which determine the ageostrophic part of the flow:

$$(hU)_x + W_y = 0$$

$$U_y - W_x = -2F.$$

Here $U \equiv -d_g v_g/dt$, $W \equiv d_g z/dt$, $F = \partial(v_g, u_g)/\partial(x, y)$, and $d_g/dt \equiv d/dt - u_a\partial/\partial x$ (the time derivative following the geostrophic motion). Hence, the ageostrophic component u_a is available diagnostically by solving

$$S_{xx} + (h^{-1}S_y)_y = -2F \tag{16}$$

for S, where $S_y = hU = z_y u_a$ and $S_x = -W$. Since $d\bar{u}/dy = h$, one has $F \approx hv_{gx}$ at small amplitude. In that limit, W (here scaled by $fH/\mathrm{Ri}^{1/2}$) is the ordinary vertical velocity in z coordinates.

We mention in appendix B how to alter the numerical model to solve (15) and (16) instead of (8) and (9). Figure 9 shows the u_g field at $t = 12$ for the case $h_0/h_1 = 1/7$ obtained using an *xyb* coordinate model. The figure includes a plot of the isentropic

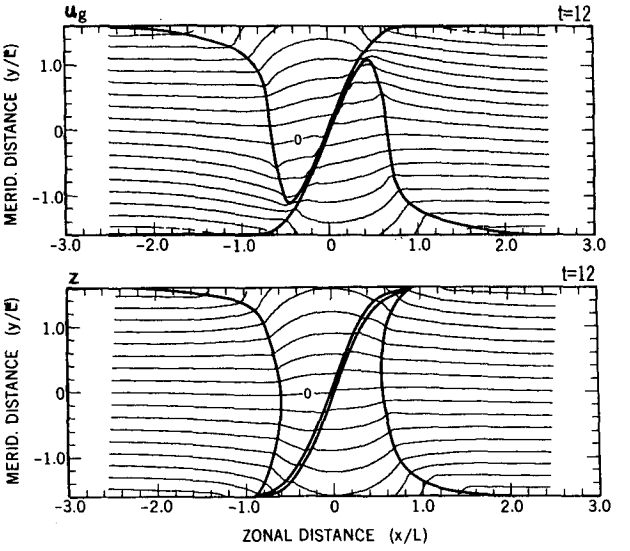

FIG. 9. Isentropic plots of (top) u_g from the isentropic model and (bottom) $z = \bar{z} + z'$ from the z-coordinate model, both at $t = 12.0$. The interpolation of $z(x, y)$ to a b surface in the bottom panel takes advantage of the constancy of $\partial b/\partial y$ and the implied identity between b and y. The wavenumber, PV ratio, and scaling are the same as for Fig. 5 except that the y axis is contracted by a factor $\mathrm{Ri}^{1/2}$. Contour intervals are $\delta u = 0.1\Delta H$ and $\delta z = 0.1H$.

height anomaly obtained by interpolating the *xyz* model solution to an isentropic surface. Theoretically, $u_g(x, y)$ is identical to the height $z(x, y)$ of a b surface. Discrepancies here are due to the different zonal resolutions in the models and to the fact that the *xyb* solution was continued past the time when the interfaces cross the computational boundaries (violating the assumptions made in imposing the computational boundary condition).[5]

The two streamfunctions $P + \bar{P}$ and S are plotted in Fig. 10. It is clear that S is coming into phase with the PV tower and the geostrophic streamfunction P. This allows an alignment of the PV contours with the total velocity, $u = u_g + u_a$, $v = v_g$. When the alignment is complete, $\partial z/\partial t$ vanishes and the "advection" of z by the geostrophic flow becomes identical with W. Note that the PV tower is preserved by meridional deflection of the flow (v_g) in isentropic coordinates, whereas the crucial deflection is in the vertical (w) in *xyz* coordinates. In isentropic coordinates, the vertical deflection is implicit.

Advection by u_a is peculiar to the baroclinic model. Its effect is always to tighten the folds of the interfaces, since these develop in regions where $\partial u_a/\partial x < 0$. The

[5] Working in isentropic coordinates suffers the disadvantage that horizontal resolution does not collapse with disturbance scales as in geostrophic coordinates. The vertical resolution is generally improved, but that advantage is offset by the need for more distant computational boundaries to contain the disturbance in the y direction.

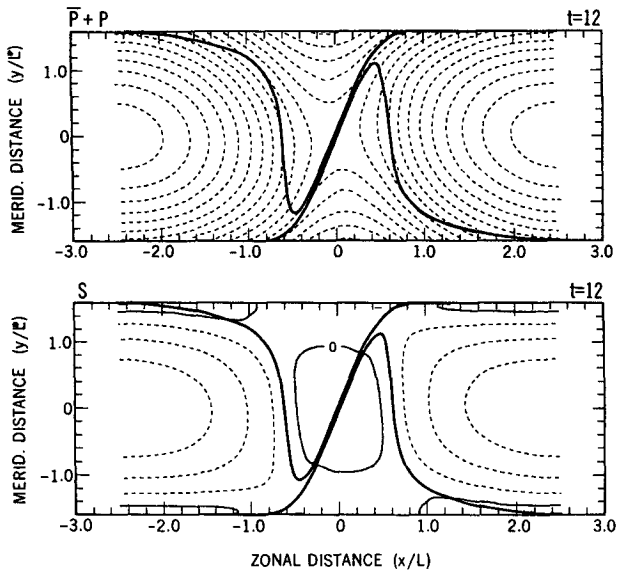

FIG. 10. Isentropic plots of (top) total geostrophic streamfunction $\bar{P} + P$ and (bottom) ageostrophic "streamfunction" S for the same time and parameters as in Fig. 9. The solution is obtained directly from the isentropic model. Contour intervals are $\delta P = 0.1(q_0/f)H^2$ and $\delta S = 0.1\Lambda H^2$.

other peculiarity is the variable coefficient in (15), which produces a stiffness in the response to PV anomalies when variations of h are O(1). In the isentropic formulation, the stiffness shows up not in the y displacements, but in the responsiveness of the z field. From inspection of (15), the nondimensional zonal scales of the intrusions must be comparable to $\sqrt{h_1/h_0}$ before the slope $z_y = -(\bar{P} + P)_{yy}$ can vary significantly within the intrusions. This means that in stiff cases, there is little vertical motion in the PV tongues until they become very narrow. In the Eady limit, the tongues must collapse to filaments (and discontinuities must form) before they can come unstuck from the boundaries.

Vertical PV advection (relative to z) is implicit in isentropic models, regardless of how the explicit ageostrophic advection is treated (e.g., McWilliams and Gent 1980). This suggests that there are alternatives to the SG model for studying finite-amplitude equilibration. If one makes the usual QG decision to neglect ageostrophic advection and basic PV variations along geostrophic trajectories, one gets a model with linearized isentropic vorticity and continuity equations that conserves the quantity

$$q_{qg} = (v'_g)_x - (z')_b.$$

Here, z' is the *small* departure from mean isentropic height. The diagnostic problem in the "isentropic QG" model is therefore like (15) but with constant coefficients. Unlike the standard, z-coordinate QG model, it would predict equilibration, though it still differs from the barotropic model because large PV variations are excluded. We have used the SG model in this study in order to keep convergence feedback in the vorticity generation and to allow strong vertical PV variations.

4. Discussion

Nakamura and Held (1989) emphasized diffusion as an ingredient in two-dimensional wave equilibration. Here we have found that by resolving the two large-PV "reservoirs" that are implicit in the standard Eady model, the role of diffusion can be eliminated without changing the life cycles in any significant way. It has been necessary to replace the equilibration scenario proposed by NH with an interpretation involving PV rollup. PV rollup is still different from the essentially dissipative processes of equilibration suggested by Orlanski (1986) and Blumen (1990). We will say more about Blumen's model shortly.

Over a full wavelength, the total PV source reduces to contributions from horizontal boundaries, namely,

$$\frac{\partial}{\partial t}\int_{-H/2}^{H/2}\int_{-L}^{L} q\,dx\,dz = \int_{-L}^{L}(f + v_x)\mathscr{H}\Big|_{-H/2}^{H/2} dx,$$

where $\mathscr{H}$ is the diffusive heating and cooling. In a primitive equation model like the one that produced Fig. 1, the net source is positive because the warm air pinches off at the lower boundary and the cold air pinches off at the upper boundary (essentially owing to the scale dependence of $\mathscr{H}$ rather than the factor $f + v_x$ which is offset by the relative widths of the heated and cooled regions). Vertical advection combines with a little interior horizontal mixing to redistribute the PV along the deepening occlusion. The similarity in the structure and behavior of the PV anomalies between the diffusive and nondiffusive numerical solutions suggests that the major role of diffusion is simply to give resolution to frontal discontinuities as PV structures.

In our nondiffusive model, potential vorticity "tongues" are fully resolved and grow entirely through advection. This process is probably not fundamentally different from the extension of the frontal discontinuity by adiabatic processes in the Eady limit. Cho and Koshyk (1989) developed an analytical model for the balanced, nondiffusive extension of a surface of discontinuity when the frontogenetical forcing consists of horizontal confluence. The analogous Eady-wave solution is evidently more complicated to obtain, and computational constraints keep us from looking at the Eady limit in our balanced numerical model. We can note, however, that in the primitive equation solution shown in Fig. 1, the vertical extent of the first PV contour is well predicted between $t = 24f^{-1}$ and $t = 36f^{-1}$ by using the average vertical velocity, $w \approx 0.05fH$, near the top of the PV intrusion during the period. The interior PV evolution thus appears to be primarily advective in that model.

With the aim of studying Eady waves after the time of nondiffusive frontal collapse, Blumen (1990) de-

veloped an analytical model of frontogenesis with implicit heat and momentum sources. The dynamics of his model are contained in surrogate momentum and thermodynamic equations [his (6), (9), (19), and (A18)] and an asymptotic matching condition. Since these are not related in a simple way to standard momentum and thermodynamic equations, we do not know the exact nature of the underlying sources of momentum and heat. However, it is clear from inspection of his Figs. 2 and 3 that large values of potential vorticity develop in the frontal region. The model actually reverses the sign of the vertical stratification anomaly in the frontal zone (from negative to positive), while retaining large values of cyclonic shear. This "occlusion" process necessarily generates large positive PV anomalies.

The PV generation in Blumen's model captures qualitatively the process occurring in primitive equation gridpoint simulations. However, his solution does not "equilibrate" in the same way: the structure of the PV anomaly retains a phase tilt for all time and the wave continues to grow exponentially outside the diffusive regions. In numerical solutions with rigid boundaries and diffusion, considerable displacement of the PV concentrations occurs, always in the direction of u and w. Cho and Koshyk's solution also suggests that rotation or lateral movement of the front cannot be avoided if the full conservation constraints are retained.

The discrepancy between the models is apparently related to the arbitrariness of the asymptotic matching condition used by Blumen to position the frontal regions. In contrast to Cho and Koshyk's (1989) method, the position of a front, say $X = X_f(Z, T)$, is a free parameter in Blumen's model, within certain bounds similar to those discussed by Cho and Koshyk in connection with their Fig. 3. Blumen's decision to fix X_f for all time (deliberately preserving the inviscid wave geometry) may imply an unusual choice for the ratio or distribution of the diffusivities of heat and momentum. We still expect wave equilibration in models that use conventional mixing parameterizations (based on comparable downgradient fluxes of heat and momentum) to resemble the nondiffusive process represented in the model with resolved PV intrusions.

A two-dimensional simulation of cyclogenesis exaggerates the importance of surface diffusion, not only by prolonging the growth, but also by highly correlating vorticity (hence horizontal scale) with temperature anomaly. A realistic alternative to diffusive surface cooling as a source of PV is elevated warming due to condensation. Condensation is always tied to the vertical motion field and does not depend on the nature of the frontogenetical forcing. Thanks to this further PV source in nature, surface "intrusions" may well be as common in the atmosphere as stratospheric intrusions. Joly and Thorpe (1990) studied the growth of disturbances on strips of positive PV anomaly produced by low-level condensation. Although the *net* PV source due to interior nonadiabatic effects must be zero, the PV tongues in their simulations and cited case studies bear a resemblance to those produced by diffusive mixing of temperature in a frontal occlusion.

Our interpretation of the two-dimensional model with resolved PV reservoirs provides an alternative view of stratospheric intrusions and PV generation at a surface front. At least in the two-dimensional framework, these PV structures can be viewed as a manifestation of the roll-up of the troposphere! Although two-dimensional models are bound to produce caricatures of midlatitude cyclones, the picture that has emerged may help in interpreting the effect of strong vertical PV variations and boundary sources on baroclinic wave equilibration in three dimensions.

Acknowledgments. We thank I. Orlanski, B. Gross, D. Dritschel, and the reviewers for their helpful comments and suggestions.

APPENDIX A

Normal Modes in the Linearized Three-Regime Models

The nondimensional streamfunction equations (15) and (4) can be written simultaneously as

$$\hat{\gamma} P_{xx} + P_{yy} = -\gamma', \qquad \text{(A1)}$$

where γ represents h or $-\zeta$ and $\hat{\gamma}$ stands for h or 1 in the respective models. For normal modes, $\gamma' = 0$ except at the internal boundaries. There the perturbation

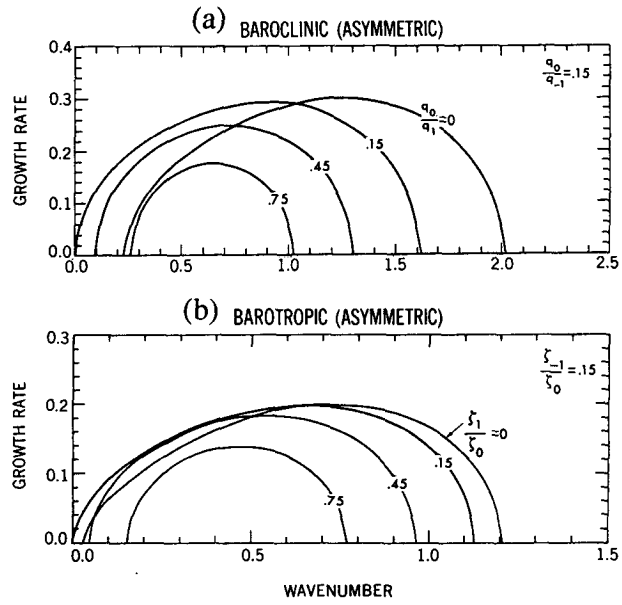

FIG. 11. Growth rate vs wavenumber in the nonsymmetric (a) baroclinic and (b) barotropic three-regime models for different values of one of the inner-to-outer vorticity or PV ratios. The other ratio is held fixed at 0.15. The phase speed (not shown) is independent of wavenumber for the unstable modes, but does depend on the ratio of the two outer values of vorticity or PV.

streamfunction P must be continuous and satisfy the linearized matching condition

$$(\partial/\partial t + y\partial/\partial x)\eta = P_x, \quad y = \pm\tfrac{1}{2}, \qquad \text{(A2)}$$

where $\eta \equiv \Delta(P_y)/\Delta\gamma$. For example, $\eta = -\Delta z'/\Delta\bar{z}_y$ in the baroclinic problem [cf. (7)].

We define $A_{\pm 1} \equiv 1 - \gamma_{\pm 1}/\gamma_0$ and $\alpha_{\pm 1}^2 \equiv \hat{\gamma}_{\pm 1}/\hat{\gamma}_0$, where the subscripts -1, 0, and 1 refer to the lower, middle, and upper layers, respectively (cf. Fig. 2). An unstable configuration must have $A > 0$ at both interfaces, according to the theorems cited in section 2. In the baroclinic model, $A \leqslant 1$ and the limit $A = 1$ ($\alpha = 0$) corresponds to a rigid boundary. The parameter α determines the characteristic y scale in the outer regions compared to the inner region. It is always unity in the barotropic model but varies with the PV in the baroclinic model. In the limit where the PV jumps are small ($\alpha \to 1$), the two linearized models become indistinguishable.

Normal-mode solutions of (A1) have the form $P(x, y, t) = \tilde{P}(y)\exp[i(kx - \omega t)]$, where

$$\tilde{P} = \begin{cases} a\sinh(ky) + b\cosh(ky), & |y| \leqslant \frac{1}{2} \\ \left[\pm a\sinh\frac{k}{2} + b\cosh\frac{k}{2}\right] \\ \quad \times \exp\left[-\alpha_{\pm 1}k\left(|y| - \frac{1}{2}\right)\right], & |y| \geqslant \frac{1}{2}. \end{cases} \qquad \text{(A3)}$$

Hence, if the interface "displacements" are $\eta_{\pm 1}(x, t) = \tilde{\eta}_{\pm 1}\exp[i(kx - \omega t)]$, one has

$$\tilde{\eta}_{\pm 1} = \frac{k}{A_{\pm 1}}\left\{a\cosh\frac{k}{2} \pm b\sinh\frac{k}{2} + \alpha_{\pm 1}\left[a\sinh\frac{k}{2} \pm b\cosh\frac{k}{2}\right]\right\}. \qquad \text{(A4)}$$

Substitution of (A4) into (A2) yields the condition

$$\frac{a}{b}\tanh\frac{k}{2} = \frac{\omega\left(\tanh\frac{k}{2} + \bar{\alpha}\right) + \left(\hat{A} - \frac{k}{2}\hat{\alpha}\right)}{\frac{k}{2}\left(\coth\frac{k}{2} + \bar{\alpha}\right) - \bar{A} - \omega\hat{\alpha}} = \frac{\frac{k}{2}\left(\tanh\frac{k}{2} + \bar{\alpha}\right) - \bar{A} - \omega\hat{\alpha}}{\omega\left(\coth\frac{k}{2} + \bar{\alpha}\right) + \left(\hat{A} - \frac{k}{2}\hat{\alpha}\right)}, \qquad \text{(A5)}$$

where the overbar and hat refer to half the sum and half the difference, respectively, of quantities in the upper and lower layers.

Frequencies ω that satisfy the second equality in (A5) come in pairs, $\omega_r + i\omega_i$ and $\omega_r - i\omega_i$, where ω_r is real and ω_i is real or imaginary. The second equality in (A5) implies that $\omega_r = -\hat{A}/(2\bar{\alpha})$ and

$$\omega_i^2 = A_\mp\frac{k(\coth k + \alpha_{\pm 1}) - A_{\pm 1}}{1 + 2\bar{\alpha}\coth k + \alpha_1\alpha_{-1}} - \left(\frac{k}{2} \pm \omega_r\right)^2. \qquad \text{(A6)}$$

The choice of sign has no effect. Notice that ω_r is independent of wavenumber. The baroclinic model has $\omega_r = \hat{\alpha} = \frac{1}{2}(\sqrt{q_0/q_1} - \sqrt{q_0/q_{-1}})$. If the right-hand side of (A6) is positive, ω_i is the growth or decay rate; otherwise, the two modes are neutral for the given wavenumber. Growth rates for symmetric configurations and different values of γ_1/γ_0 are graphed as a function of wavenumber in Fig. 4. Growth rates for several asymmetric cases with one of the ratios fixed at 0.15 are graphed in Fig. 11. Notice the appearance of a long-wave cutoff in the asymmetric cases ($\gamma_{-1} \neq \gamma_1$ and $\omega_r \neq 0$). In the small-k limit, the right-hand side of (A6) is approximately $Bk - \omega_r^2$, where $B = (\bar{A} - A_1A_{-1})/(2\bar{\alpha})$. A long-wave cutoff therefore appears near $k = \omega_r^2/B$. The stabilization at small wavenumber is similar to the effect of a planetary vorticity gradient on long Rossby waves.

The steering level, say $y = y_s$, is defined by $\bar{u}(y_s) = c_r$, where c_r is the real part of the phase speed. Hence, $y_s = \omega_r/k$ in the unstable modes. In both types of models, the steering level for unstable modes is at middepth in symmetric cases (since $\omega_r = 0$ when $\gamma_{-1} = \gamma_1$), but otherwise is closer to the interface that has the smaller contrast in vorticity or PV (wherever γ/γ_0 is larger). In Eady's (1949) example with infinite lower-level PV ($\gamma_{-1} = 0$) and finite upper-level PV, the unstable modes move in the direction of the upper-level flow. The steering level shifts toward the interface with the smaller PV jump because the propagation of edge waves against the mean flow is weaker there.

APPENDIX B

Outline of Numerical Solution Procedure

Here we describe our method for solving the elliptic problems (8) and (9). Since q_{sg} is a coefficient in the equations and may be a function of X, we use finite differences in both the horizontal and the vertical. We use the direct elliptic solver (called "EVP") described by Roache (1976). Since the differencing is straightforward, we concentrate here on the implementation of the open boundary condition at the top and bottom of the computational domain.

If we define a variable $A(X, Z)$ such that $\partial A/\partial X = \chi$, then (8) and (9) are of the same form, namely,

$$q_{sg}A_{XX} + A_{ZZ} = F, \qquad \text{(B1)}$$

where the variables are nondimensional. The xyb-coordinate problems (15) and (16) also have this form if we define $\partial A/\partial y = S$ and identify y with Z. We assume that the forcing $F(X, Z)$ vanishes outside the computational boundaries, say in $|Z| > Z_b$. This is exactly true of (8) and (15) if the boundaries are placed far enough outside $Z = \pm\frac{1}{2}$, since we are using discrete distributions of q_{sg}. However, since the forcing in (9) and (16) is not exactly zero at the boundaries, an ex-

ponentially small error is introduced when solving for the ageostrophic streamfunction.

With the assumption about $F(X, Z)$, the solution of (B1) in $|Z| > Z_b$ can be represented by the Fourier series

$$A(X_n, Z) = \sum_{m=-M}^{M} \tilde{A}_m(Z_b) \exp(ik_m X_n) \times \exp(-\alpha|k_m(Z - Z_b)|), \quad \text{(B2)}$$

where $\tilde{A}(Z)$ is the discrete transform of A over the $2M$ grid points in X and $\alpha \equiv \sqrt{q_{\pm 1}}$. The discrete wavenumbers are $k_m \equiv m\pi/L$, where L is half the width of the periodic domain. Choosing the outwardly damped vertical structure for each horizontal scale ensures boundedness at infinity.

A linear relation between the solution at $Z = Z_b$ and the solution at $Z = Z'_b$ (one grid point away) is obtained by evaluating (B2) at $Z = Z'_b$. With the help of the convolution theorem, the result is expressed as a sum over the grid points X_n,

$$A(X_n, Z'_b) = \sum_{m=-M}^{M} A(X_m, Z_b) B(X_m - X_n) \Delta X;$$

$$B(X) = \frac{1}{L} \operatorname{Re}\left\{\frac{1 - \exp[(M+1)k_1(iX - \alpha\Delta Z)]}{1 - \exp[k_1(iX - \alpha\Delta Z)]}\right\}, \quad \text{(B3)}$$

where $\Delta X = L/M$ and $\Delta Z \equiv |Z_b - Z'_b|$. The expression named $B(X)$ is the inverse transform of $\exp(-\alpha|k_n|\Delta Z)$. Typically, M is large enough to make the second term in the numerator negligible, and one finds that

$$B(X) \approx \frac{1}{\pi} \frac{\frac{2}{k_1}\left[\sinh\left(\frac{k_1}{2}\alpha\Delta Z\right)\exp\left(\frac{k_1}{2}\alpha\Delta Z\right) + \sin^2\left(\frac{k_1}{2}X\right)\right]}{\frac{4}{k_1^2}\left[\sinh^2\left(\frac{k_1}{2}\alpha\Delta Z\right) + \sin^2\left(\frac{k_1}{2}X\right)\right]}. \quad \text{(B4)}$$

If L is big enough that $|X|/L \ll 1$ in the region of the forcing, and $\alpha\Delta Z/L$ is also small, one has the further approximation

$$B(X) \approx \frac{1}{\pi} \frac{\alpha\Delta Z}{(\alpha\Delta Z)^2 + X^2}, \quad \text{(B5)}$$

which is the continuous inverse transform of $\exp(-\alpha|k|\Delta Z)$. Once B is evaluated for discrete values of X, the linear relation (B3) can be incorporated into the direct solver as a boundary condition. Notice that the limit $\alpha \to 0$ yields $B \to \delta(X)$ (Dirac delta). This limit corresponds to the Neumann boundary condition, $A(X, Z'_b) = A(X, Z_b)$. The limit $\alpha \to \infty$ yields the Dirichlet condition, $A(X, Z'_b) = 0$.

REFERENCES

Blumen, W. A., 1980: On the evolution and interaction of short and long baroclinic waves of the Eady type. *J. Atmos. Sci.*, **37**, 1984–1993.

——, 1990: A semigeostrophic Eady-wave frontal model incorporating momentum diffusion. Part I: Model and solutions. *J. Atmos. Sci.*, **47**, 2890–2902.

Charney, J. G., and M. E. Stern, 1962: On the stability of internal baroclinic jets in a rotating atmosphere. *J. Atmos. Sci.*, **19**, 159–172.

Cho, H.-R., and J. N. Koshyk, 1989: Dynamics of frontal discontinuities in the semigeostrophic theory. *J. Atmos. Sci.*, **46**, 2166–2177.

Dritschel, D. G., 1988: The repeated filamentation of two-dimensional vorticity interfaces. *J. Fluid Mech.*, **194**, 511–547.

Eady, E. J., 1949: Long waves and cyclones waves. *Tellus*, **1**, 33–52.

Fjørtoft, R., 1950: Application of integral theorems in deriving criteria of stability for laminar flows and for the baroclinic circular vortex. *Geofys. Publ.*, **17**(6), 1–52.

Gall, R. L., 1976: Structural changes of growing baroclinic waves. *J. Atmos. Sci.*, **33**, 374–390.

Hirschberg, P. A., and J. M. Fritsch, 1991: Tropopause undulations and the development of extratropical cyclones. Part I: overview and observations from a cyclone event. *Mon. Wea. Rev.*, **119**, 496–517.

Hoskins, B. J., 1975: The geostrophic momentum approximation and the semigeostrophic equations. *J. Atmos. Sci.*, **32**, 233–242.

——, and F. P. Bretherton, 1972: Atmospheric frontogenesis models: Mathematical formulation and solution. *J. Atmos. Sci.*, **29**, 11–37.

——, and A. A. Draghici, 1977: The forcing of ageostrophic motion according to the semigeostrophic equations and in an isentropic coordinate model. *J. Atmos. Sci.*, **34**, 1859–1867.

——, M. E. McIntyre, and A. W. Robertson, 1985: On the use and significance of isentropic potential vorticity maps. *Quart. J. Roy. Meteor. Soc.*, **111**, 877–946.

Joly, A., and A. J. Thorpe, 1990: Frontal instability generated by tropospheric potential vorticity anomalies. *Quart. J. Roy. Meteor. Soc.*, **116**, 525–560.

McWilliams, J. C., and P. R. Gent, 1980: Intermediate models of planetary circulations in the atmosphere and ocean. *J. Atmos. Sci.*, **37**, 1657–1678.

Magnusdottir, G., and W. H. Schubert, 1990: The generalization of semigeostrophic theory to the β plane. *J. Atmos. Sci.*, **47**, 1714–1720.

Nakamura, N., and I. M. Held, 1989: Nonlinear equilibration of two-dimensional Eady waves. *J. Atmos. Sci.*, **46**, 3055–3064.

Orlanski, I., 1986: Localized baroclinicity: A source for meso-α cyclones. *J. Atmos. Sci.*, **43**, 2857–2885.

Pedlosky, J., 1987: *Geophysical Fluid Dynamics.* Springer-Verlag, 710 pp.

Pozrikidis, P., and J. J. L. Higdon, 1985: Nonlinear Kelvin–Helmoltz instability of a finite vortex layer. *J. Fluid Mech.*, **157**, 225–263.

Rayleigh, L., 1894: *The Theory of Sound,* 2nd ed. Macmillan, 999 pp.

Roache, P. J., 1976: Basic computational methods for incompressible flow. *Computational Fluid Dynamics,* Hermosa, chapter 3.

Sakai, S., 1989: Rossby–Kelvin instability: a new type of ageostrophic instability caused by a resonance between Rossby waves and gravity waves. *J. Fluid Mech.*, **202**, 149–176.